Accepted Manuscript
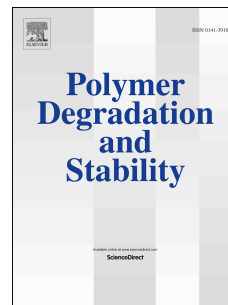
Measuring method for thermal conductivity of a pyrolysis layer

Jin Guo, Haiming Huang, Qing Wang, Ye Tian, Yipu Zhao

Please cite this article as: Guo J, Huang H, Wang Q, Tian Y, Zhao Y, Measuring method for thermal conductivity of a pyrolysis layer, *Polymer Degradation and Stability* (2019), doi: https://doi.org/10.1016/j.polymdegradstab.2019.05.035.

Measuring method for thermal conductivity of a pyrolysis layer

Jin Guo[1], Haiming Huang[1*], Qing Wang[2], Ye Tian[1], Yipu Zhao[1]

1. Institute of Engineering Mechanics, Beijing Jiaotong University, Beijing, 100044, China

2. Department of Engineering, Durham University, Durham, United Kingdom

* Corresponding author: huanghaiming@tsinghua.org.cn

Abstract

The thermo-physical parameters of the pyrolysis layer in charring material play a fundamental role in the design of the thermal protection system (TPS) in hypersonic vehicles, but there is still a lack of measuring methods for the pyrolysis layer including pyrolysis gases, carbon residue and resin. The measuring method for the thermal conductivity of the pyrolysis layer is presented by means of iteration inversion of temperature at measuring points, and experimental equipment is designed and manufactured. Furthermore, the thermal conductivity of the pyrolysis layer under different pressures is obtained by this method. The results reveal that its thermal conductivity is a nonlinear function of temperature; meanwhile, the pressure has a major effect on the thermal conductivity. This study can figure out the test problem of the thermal conductivity of the pyrolysis layer, which is helpful to the optimization of TPS.

Keywords: Measuring method; Experimental equipment; Thermal conductivity;

Pyrolysis layer; Pressure

ACCEPTED MANUSCRIPT

Nomenclature

c_p	specific heat [J·kg^{-1}·K^{-1}]	*Subscripts*	
h	enthalpy [J·kg^{-1}]	c	interface between the pyrolysis layer and the char layer
J	Jacobian matrix [-]		
k	thermal conductivity [W·m^{-1}·K^{-1}]	cal	calculated results
		exp	experimental results
L	material thickness [m]	g	the pyrolysis gas
L_t	distance between middle test point and material bondline [m]	m	parameter at temperature T_m
		p	interface between the virgin layerand the pyrolysis layer
m	mass [kg]	w	surface
R	temperature difference [K]	0	initial value
T	temperature [K]	00	initial value
t	time [s]	1	the virgin layer
x	space coordinate [m]	2	the pyrolysis layer
γ	convergence error [-]	3	the char layer
λ	damping coefficient [-]		
ρ	density [kg·m^{-3}]		

1. Introduction

The use of thermal protection systems (TPS) is required during atmosphere entry missions in order to mitigate the aerothermal loads experienced at hypersonic conditions [1]. Charring material such as phenolic-impregnated carbon ablators is one successful class of TPS materials [2-4], and its thermo-physical parameters are crucial for the design of the TPS [5-7]. When simulating the thermal response of the charring material, the thermo-physical parameters are indispensable no matter what method we use [8-11]. Currently, thermal conductivity of the pyrolysis layer is usually approximated by the linear interpolation of that in the virgin layer and in the char layer, respectively, when using the pyrolysis layer model to simulate the thermal response of the charring material [12-15]. This approximation makes the TPS partial to safety, but it's not good for optimization.

For the optimization of the TPS, it is necessary to obtain actual thermal conductivity of the pyrolysis layer, which is composed of the resin carbonization, the flow of the pyrolysis gases and the carbon fibers [16-21]. Actually, it changes with temperature and is hard to measure [22-24]. Over the last decade, a few researchers have explored this problem. For example, thermal diffusivity, measured as a function of temperature from 15 $^{\circ}$C to 50 $^{\circ}$C, is taken to calculate the bondline temperature of the carbon fiber reinforced epoxy resins during pyrolysis [25], but the measured parameter is not thermal diffusivity of the pyrolysis layer. Bourbigot et al. [26] measured the thermal conductivity of intumescent coatings using hot disc equipment

(TPS2500, Sweden), but TPS2500 measures the effective thermal conductivity of the whole sample. Up to now, it is difficult to measure the thermal conductivity of the pyrolysis layer and there is still a lack of measuring methods for the pyrolysis layer.

Therefore, a measuring method is presented in order to obtain thermal conductivity of the pyrolysis layer by means of iteration inversion of temperature at measuring points, and the experimental equipment is designed and manufactured to realize this measurement method.

2. Experimental design

The specimen is prepared in sequence by vacuum-impregnation, drying, curing, and cooling processes in turn by our group [3, 4]. In addition, the cross section of the specimen is a square of 0.1 m×0.1 m.

In order to acquire the thermal response of the pyrolysis layer under different pressures, experimental equipment is designed and manufactured, as shown in Fig.1 (a). The schematic configuration of the equipment is presented in Fig. 1 (b) and it consists of the measuring system, the test system, the specimen delivery system and the pneumatic control system. The test system is the main measuring unit of this experimental equipment and it consists of the specimen (1), the alumina insulating firebrick (2), the heating element (3) and the hot plate (4). It can be observed that there is a gap between the heating element and the hot plate in order to make the heat more uniform. The hot plate made of SiC is situated closely next to the specimen. The specimen is heated by the hot plate; in addition, the sides and the back of the

specimen are filled with the alumina insulating firebrick; therefore, the heat conduction is assumed to be one-dimensional. During the experiment, the air pressure is controlled by the pneumatic control system, consisting of the air inlet (5), the air outlet (6), the pneumatic valve (7) and the vacuum tank (8). The air flows into this experimental equipment by air inlet and flows out by air outlet. When the air pressure inside the equipment measured by the pneumatic valve is steady, the heating element is turned on and the hot plate is heated by the heating element. When the temperature of the hot plate measured by thermocouples is steady at a certain temperature (T_c), the specimen is transported to the designated position by the specimen delivery system. This specimen delivery system consists of the specimen tray (9), bearing rod (10) and the motor starter (11). When the specimen reaches the designated position, the upper surface of the specimen is in close contact with the hot plate. There is a pressure sensor at the specimen tray, and when the pressure is high enough, the contact area of the hot plate and the specimen is considered complete. The thermal response of the specimen under different pressures is recorded by the measuring system. There are thermocouples (12) installed at the hot plate, the middle test point and the bondline, besides, the temperatures of these three test points are recorded by the installed thermocouples after each 30-second exposure. There are five thermocouples, four thermocouples, and five thermocouples installed at the bondline, the middle test point, and the hot plate, respectively, as presented in Fig. 2. The final experimental results at each test point are the average of the results recorded by different thermocouples.

(a)
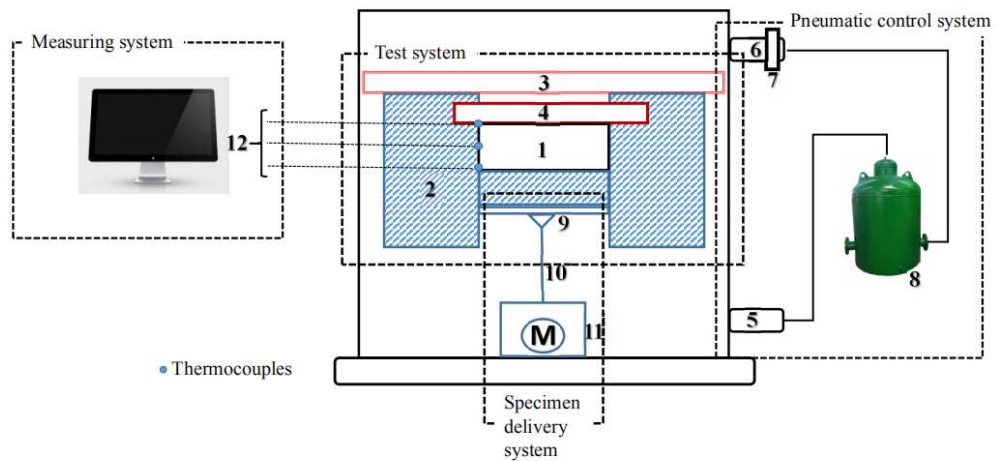
1. Specimen 2. Alumina insulating firebrick 3. Heating element 4. Hot plate
5. Air inlet 6. Air outlet 7. Pneumatic valve 8. Vacuum tank 9. Specimen tray
10. Bearing rod 11. Motor starter 12. Thermocouples

(b)

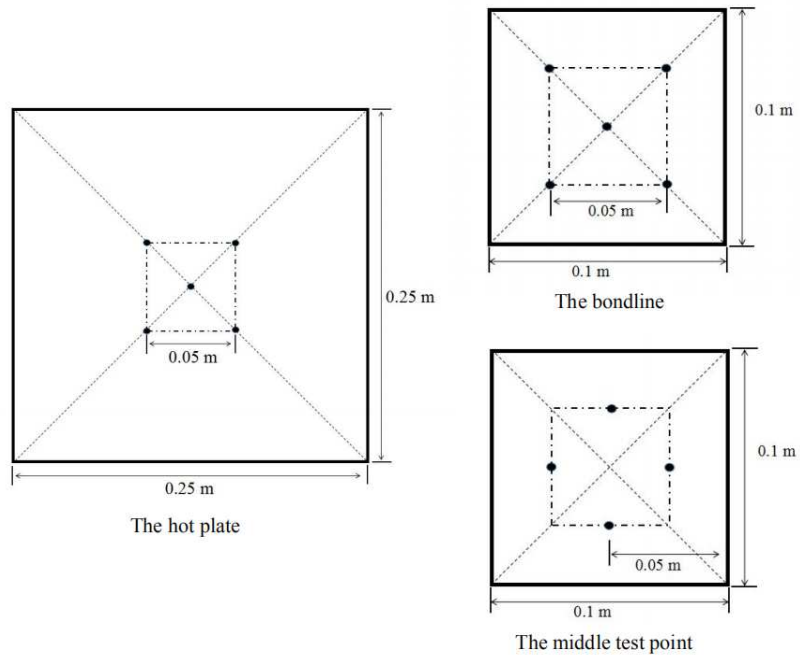Fig. 1. (a) Experimental equipment and (b) its schematic configuration

Fig. 2. Distributions of the thermocouples at the hot plate, the bondline and the middle

test point

3. Measuring method based on experimental results

The temperatures of the bondline and the heating surface can be measured by the

experimental equipment (Fig. 1), and then the thermal conductivity of the pyrolysis

layer can be obtained using the iteration inversion method based on the pyrolysis

layer model.

3.1. The pyrolysis layer model

The pyrolysis layer model is taken to predict the thermal behavior of the charring

material. The pyrolysis layer model has been validated with experimental data in the

study of our group in ref. [13]. The pyrolysis layer model consists of three layers: the

virgin layer, the pyrolysis layer and the char layer. During the heating process, the

charring material undergoes thermal degradation. A variety of physical and chemical

phenomena are involved, and the overall material response can be described by the pyrolysis of solid resin and the transport of pyrolysis gases through porous char [18-21]. Under the external heat load, part heat is absorbed by the charring material, and then if the temperature on the surface reaches the start pyrolysis temperature T_p, the resin begins to pyrolyze and the pyrolysis layer forms. The char layer does not appear until the temperature at the material surface reaches the full pyrolysis temperature T_c, so there are the virgin layer and the pyrolysis layer in the specimen if the temperature at the heating surface is kept at T_c. Once the temperature at the bondline reaches the start pyrolysis temperature T_p, the experiment is stopped and there only remains the pyrolysis layer at the end of the experiment, as shown in Fig. 3. Coordinates 0, x_p, and L are respectively the bondline, the interface between the virgin layer and the pyrolysis layer, and the heating surface. T_w is the wall temperature and it is equal to T_c in this experiment.
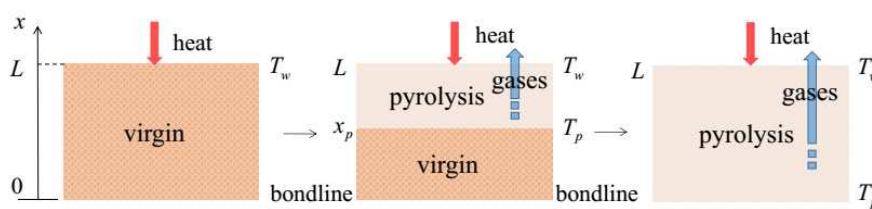

Fig. 3. Pyrolysis of the charring material during the experiment

Here are some assumptions in the pyrolysis layer model

(a) There is no secondary cracking for pyrolysis gases and the pyrolysis gases do not react with the carbon fiber.

(b) There is no energy exchange between the pyrolysis gases and the solid material.

(c) The volume change caused by the pyrolysis gases accumulation is neglected.

The above model is expressed by the following differential equations

$$\rho_1 c_{p1} \frac{\partial T(x,t)}{\partial t} = \frac{\partial}{\partial x}[k_1 \frac{\partial T(x,t)}{\partial x}] \qquad\qquad 0 \le x < x_p \qquad (1)$$

$$\rho_2 c_{p2} \frac{\partial T(x,t)}{\partial t} = \frac{\partial}{\partial x}[k_2 \frac{\partial T(x,t)}{\partial x}] + \dot{m}_{g2} c_{pg} \frac{\partial T(x,t)}{\partial x} + \frac{\partial \rho_2}{\partial t} h_g \qquad x_p \le x < L \qquad (2)$$

where ρ, c_p, k are respectively the density, the specific heat, the thermal conductivity, and h is the pyrolysis gases enthalpy. $\dot{m}$ is the pyrolysis gases mass injection rate, subscript g stands for the pyrolysis gases, and subscripts 1 and 2 represent the virgin layer and the pyrolysis layer, respectively.

In the pyrolysis layer, the conservation of mass is as follow

$$\partial \rho_2 / \partial t = -d\dot{m}_{g2} / dx \qquad\qquad (3)$$

In addition, the boundary conditions are written as

$$-k_1 \frac{\partial T(x,t)}{\partial x} = 0 \qquad x = 0 \qquad\qquad (4)$$

$$T = T_p \qquad x = x_p \qquad\qquad (5)$$

$$T = T_w \qquad x = L \qquad\qquad (6)$$

The heat flux in $x = x_p$ must satisfy

$$-k_1 \frac{\partial T(x,t)}{\partial x} = -k_2 \frac{\partial T(x,t)}{\partial x} \qquad x = x_p \qquad\qquad (7)$$

The initial temperature distribution of the charring material is linear interpolated by the measured temperatures at the bondline and the middle test point at $t = 0$ s. This model is discretized using the central difference format, and solved by the MATLAB

codes in Ref. [12, 13].

3.2. Iteration inversion method

On the basis of the measured thermal response of the pyrolysis layer at different pressures, the thermal conductivity of the pyrolysis layer of the specimen under different pressures can be obtained by means of iteration inversion of temperature at measuring points. This method is calculated by the following steps:

(1) Estimate the initial values. It is assumed that $k_{m,0}^1 = (k_1+k_3)/2$ and $k_{m,00}^1 = (k_1+k_3)/2-\varepsilon$, where ε is an arbitrary value, $\varepsilon=0.1\times k_1$ in this study. Subscript m stands for the parameter at temperature T_m and $T_m = (T_p+T_c)/2$, subscript 3 stands for the char layer, subscripts 0 and 00 stand for two initial values and the superscript stands for the iteration step.

In order to inverse the thermo-physical properties of the pyrolysis layer, it must be assumed that there is a virtual node outside the heating surface (the interface between the pyrolysis layer and the char layer) of the specimen. This virtual node is close to the heating surface and the distance is the length of one grid. The thermo-physical properties at this virtual node are that of the char layer at T_c.

Parameter k_m is the thermal conductivity of the pyrolysis layer at temperature T_m. Combining the thermal conductivity of the virgin layer at T_p (the interface between the virgin layer and the pyrolysis layer) and the thermal conductivity of the char layer at T_c (the virtual node), the thermal conductivity of the pyrolysis layer is approximated as

$$k_2(T) = \frac{\dfrac{(k_1 - k_m)}{T_p - T_m} - \dfrac{(k_m - k_3)}{T_m - T_c}}{T_p - T_c} \times T^2 + \left[(\frac{(k_1 - k_m)}{T_p - T_m}) - \right. \tag{8}$$

$$\left. (T_p + T_m) \frac{\dfrac{(k_1 - k_m)}{T_p - T_m} - \dfrac{(k_m - k_3)}{T_m - T_c}}{T_p - T_c} \right] \times T + \left\{ k_1 - \frac{\dfrac{(k_1 - k_m)}{T_p - T_m} - \dfrac{(k_m - k_3)}{T_m - T_c}}{T_p - T_c} \times T_p^2 \right.$$

$$\left. - \left[(\frac{(k_1 - k_m)}{T_p - T_m}) - (T_p + T_m) \frac{\dfrac{(k_1 - k_m)}{T_p - T_m} - \dfrac{(k_m - k_3)}{T_m - T_c}}{T_p - T_c} \right] \times T_m \right\}$$

(2) On the basis of the two given initial values of k_m, two kinds of distributions of thermal conductivity of the pyrolysis layer can be calculated by Eq. (8), and then two kinds of thermal response of the charring material can be predicted by the pyrolysis layer model. Two calculated bondline temperatures are respectively marked as $T_{cal,0}^1$, $T_{cal,00}^1$ and the measured bondline temperature is marked as T_{exp}, where subscripts *cal* and *exp* stand for the calculated results and experimental results, respectively. The temperature data is recorded every 30 s, so T_{exp}, $T_{cal,0}$ and $T_{cal,00}$ are vectors of temperature.

(3) Based on the Levenberg-Marquardt algorithm [27, 28], the equation is as follow

$$(J^T J + I\lambda)\Delta k = J^T R \tag{9}$$

where *I* is the unit matrix and λ is the introduced damping coefficient for the purpose of improving the convergence of this method.

J is the Jacobian matrix

$$J^i = \left[\frac{\partial T_{cal,1}^i}{\partial k_m} \quad \frac{\partial T_{cal,2}^i}{\partial k_m} \quad ... \quad \frac{\partial T_{cal,n}^i}{\partial k_m} \right] \tag{10}$$

where n is the total time step, i is the iteration step.

Each element of the Jacobian matrix can be approximated as

$$\frac{\partial T_{cal}^{i}}{\partial k_{m}} = \frac{T_{cal}^{i}(k_{m,00}^{i}) - T_{cal}^{i}(k_{m,0}^{i})}{k_{m,00}^{i} - k_{m,0}^{i}} \tag{11}$$

In Eq. (9), R is defined by

$$R^{i} = T_{exp} - T_{cal}^{i} \tag{12}$$

From Eq. (9), we have

$$\Delta k^{i} = [(J^{i})^{T} J^{i} + I\lambda]^{-1} (J^{i})^{T} R^{i} \tag{13}$$

With the calculated Δk, two initial values of k_{m} at the i+1 iteration step can be calculated, let $k_{m,0}^{i+1} = k_{m,00}^{i}$, $k_{m,00}^{i+1} = k_{m,00}^{i} + \Delta k^{i}$.

(4) The convergence criterion is

$$\max\left(\left|\frac{k_{m,00}^{i} - k_{m,0}^{i}}{k_{m,00}^{i}}\right|\right) < \gamma \tag{14}$$

where $\gamma = 0.001$ in this study.

If this convergence criterion is satisfied then stop the iteration, $k_{m,00}^{i+1}$ is what we needed. Otherwise, if this criterion is not satisfied, return to step (2) with two newly calculated initial values of k_{m}.

4. Results and discussion

Some material properties are presented in Appendix A. The thickness of the material (L) and the distance between the middle test point and the bondline (L_t) under different pressures are listed in Table 1.

Table 1 The thickness of the material (L) and the distance between the middle test point and the material bondline (L_t) under different pressures

	L (m)	L_t (m)
101 kPa	0.02547	0.01201
50 kPa	0.02493	0.01279
4 kPa	0.02515	0.01264

The temperature profiles of the specimen at the bondline, the middle test point and the heating surface at pressures of 101, 50 and 4 kPa are plotted in Fig. 4. The temperature profiles of the heating surface under different pressures are zoomed and they are roughly stable at a certain temperature, as shown in Fig. 4. It is easy to reach the conclusion that the heating time increases with pressure decreases from 101 kPa to 4 kPa under the same bondline temperature rise. It is revealed that the overall capacity of heat transmission of the material decreases as pressure decreases. Moreover, the influence of the pressure on the capacity of heat transmission of the material at a pressure of 4 kPa is greater than that at pressures of 50 and 101 kPa.
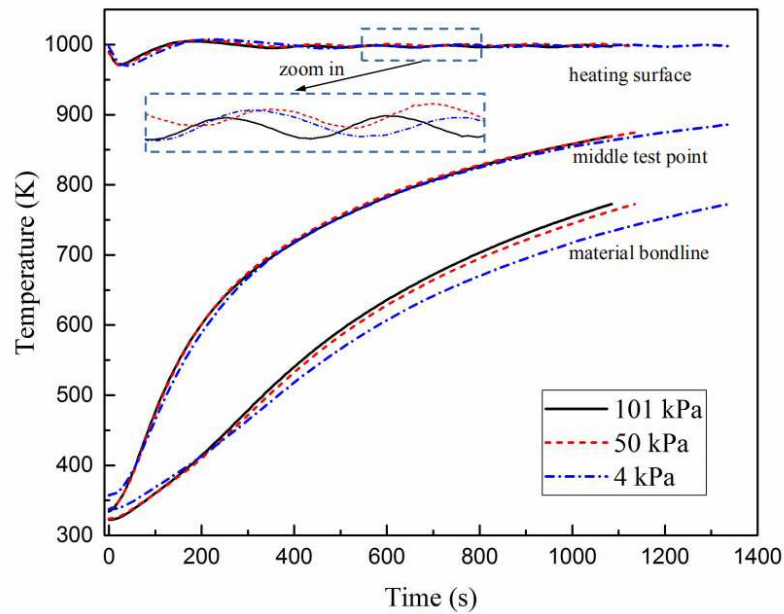
Fig. 4. Measured temperature profiles of the specimen at the bondline, the middle test

point and the heating surface at three kinds of pressure

According to the measured results by the experimental equipment, the thermal

conductivity of the pyrolysis layer at pressures of 101, 50 and 4 kPa can be obtained,

as depicted in Fig. 5. It is clear to see from Fig. 5 that the thermal conductivity

decreases as the air pressure decreases and all of them are nonlinear functions of

temperature. The thermal conductivity at a pressure of 50 kPa is slightly lower than

that at a pressure of 101 kPa; however, the thermal conductivity at a pressure of 4 kPa

is much less than that at a pressure of 101 kPa. The influence of the pressure on the

thermal conductivity of the pyrolysis layer is increasing at low pressures. The

decrease of the air pressure has no effect on the heat conduction of solid and radiation

in porous material. However, due to the high porosity of the pyrolysis layer, thermal

conductivity of the gas-phase plays an important role in the overall heat transfer. The

decrease of the air pressure has a major effect on the heat transfer of the gas-phase. In addition, the pyrolysis gases released outside during pyrolysis and the amount of pyrolysis gases released decreases with the increase of the air pressure. The amount of pyrolysis gases in the pyrolysis layer is negatively correlated with the air pressure and this leads to the decrease of thermal conductivity of the pyrolysis layer as the air pressure decreases.
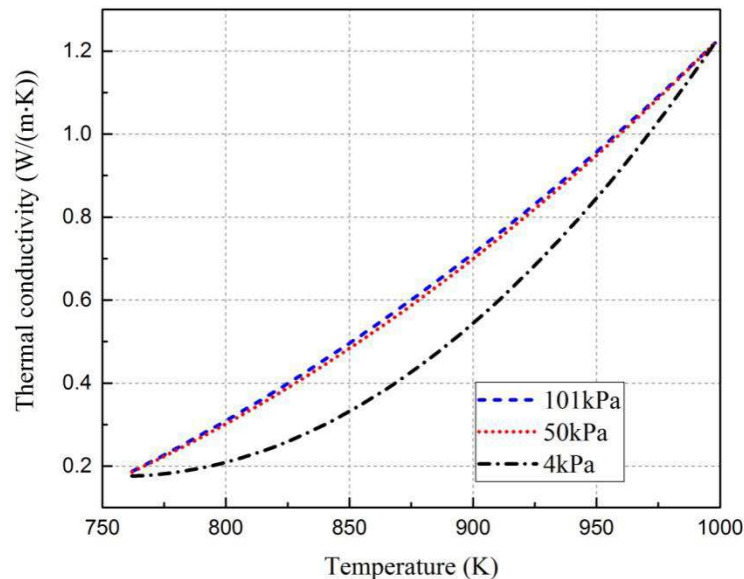

Fig. 5. Thermal conductivity of the pyrolysis layer at pressures of 101, 50 and 4 kPa

The thickness of the virgin layer, the pyrolysis layer and the char layer of the charring material during pyrolysis at pressures of 101, 50 and 4 kPa are shown in Fig. 6. The method for the estimation of the thickness of different layers has been presented in the study of our group in ref. [12]. The thickness of the virgin layer decreases with the increase of time and the thickness of the pyrolysis layer increases with the increase of time. The thickness of the char layer remains at 0, which indicates

that the char layer did not appear during the experiment. As is demonstrated in Fig. 6, the air pressure has an effect on the pyrolysis of the charring material. With the decrease in air pressure, the pyrolysis rate of the charring material decreases.
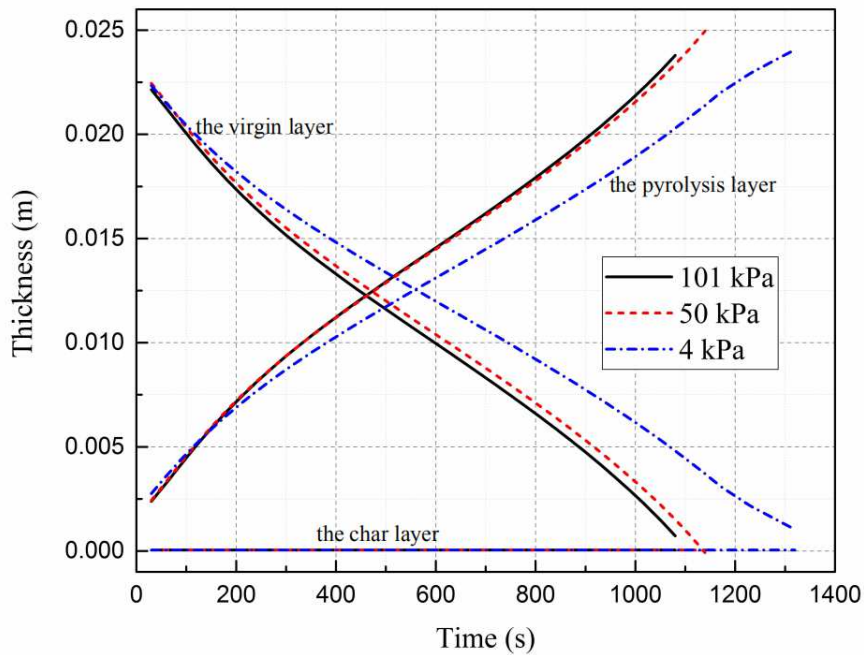

Fig. 6. Thickness of the virgin layer, the pyrolysis layer and the char layer of the charring material at pressures of 101, 50 and 4 kPa

5. Conclusions

So far, no reported experimental equipment and methods have been found to measure the thermal conductivity of pyrolysis layers, so the relationship between thermal conductivity and temperature of the pyrolysis layer has been studied here. The influence of pressure was also considered. The results indicate that

(1) Experimental equipment can be used to obtain the thermal conductivity of the pyrolysis layer under different air pressures.

(2) Thermal conductivity of the pyrolysis layer is usually approximated by the linear

interpolation of that in the virgin layer and in the char layer, respectively. However, the result that thermal conductivity of the pyrolysis layer is a nonlinear function of temperature is good for the optimization design of the thermal protection system.

(3) The air pressure has an effect on the pyrolysis of the charring material. With the decrease of the air pressure, the overall capacity of heat transmission of the material decreases.

Acknowledgment

Appendix A

In this experiment, the charring material (455 kg·m^{-3}) is prepared by impregnating carbon fiber preform (300 kg·m^{-3}) with boron modified phenolic resin anhydrous ethanol solution (without adding any filler), then dried and cured at different temperatures.

The TG and DTG curves of phenolic resin are shown in Figs. A. 1 (a) and (b). The weight loss is more than 15 % with a high weight loss rate from 300 K to 600 K, which is attributed to the curing reaction of the phenolic resin. Simultaneously, the curing reaction of the phenolic resin corresponds to the first peak of the DTG profile. The weight loss is about 20 % with a high weight loss rate from 762 K to 998 K, which is attributed to the pyrolysis process of the phenolic resin. Simultaneously, the pyrolysis process of the phenolic resin corresponds to the second peak of the DTG

profile. It is determined that the starting pyrolysis temperature of the phenolic resin is 762 K and the full pyrolysis temperature is 998 K. The thermal conductivity of the pyrolysis layer is discussed over the T in this study, and the effect of the heating rate will be studied in future work.
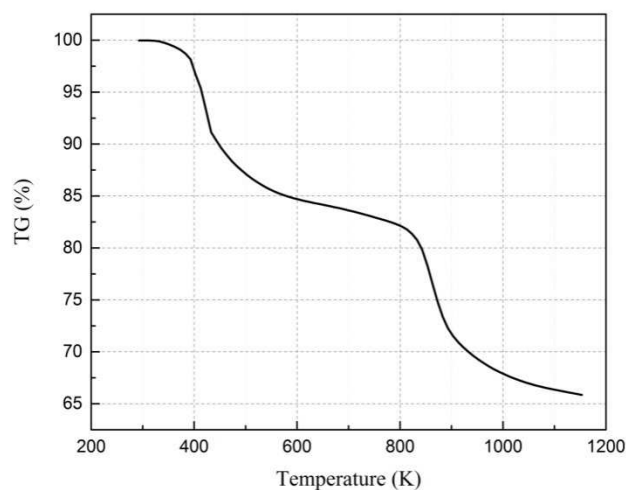
(a)
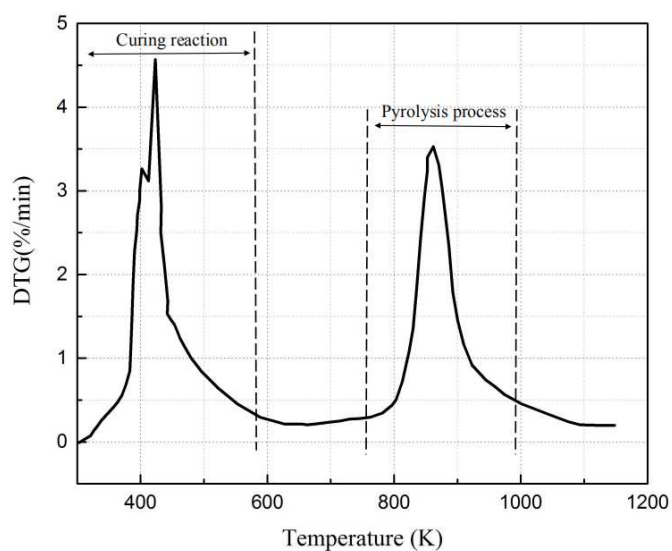
(b)

Fig. A. 1. (a) TG and (b) DTG of phenolic resin

The material properties of the charring material are given in Table A. 1. As is listed in Table A. 1, the density, thermal conductivity and specific heat of the virgin layer are constant; the density, thermal conductivity and specific heat of the char layer are also constant.

Table A. 1 Properties of the charring material

	Properties	Unit	Value
Virgin layer	Density	$kg \cdot m^{-3}$	455
	Specific heat	$J \cdot kg^{-1} \cdot K^{-1}$	770
	Thermal conductivity	$W \cdot m^{-1} \cdot K^{-1}$	0.187 (101 kPa)
	Thermal conductivity	$W \cdot m^{-1} \cdot K^{-1}$	0.186 (50 kPa)
	Thermal conductivity	$W \cdot m^{-1} \cdot K^{-1}$	0.176 (4 kPa)
Char layer	Density	$kg \cdot m^{-3}$	341
	Specific heat	$J \cdot kg^{-1} \cdot K^{-1}$	1520
	Thermal conductivity	$W \cdot m^{-1} \cdot K^{-1}$	1.22
Pyrolysis layer	Specific heat of the pyrolysis gases	$J \cdot kg^{-1} \cdot K^{-1}$	9630
	Enthalpy of the pyrolysis gases	$J \cdot kg^{-1}$	9.02×10^{6}
	The begin pyrolysis temperature	K	762
	The full pyrolysis temperature	K	998

The pyrolysis of the charring material is an internal decomposition of the solid that releases gaseous species, such as methane, carbon monoxide, carbon dioxide and hydrogen. There are chemical reactions, heat transfer, gas-phase and solid-phase in

the pyrolysis layer, the thermal diffusivity of the pyrolysis layer is hard to obtain. The density, thermal conductivity and specific heat of the pyrolysis layer show a gradient or an S-shape over the layer thickness. The density ρ_2 of the pyrolysis layer is obtained by the thermogravimetry data ϕ of the charring material

$$\rho_2(T) = \rho_1 \times \phi(T)$$
(A. 1)

The profile of the density distribution of the pyrolysis layer is shown in Fig. A. 2.
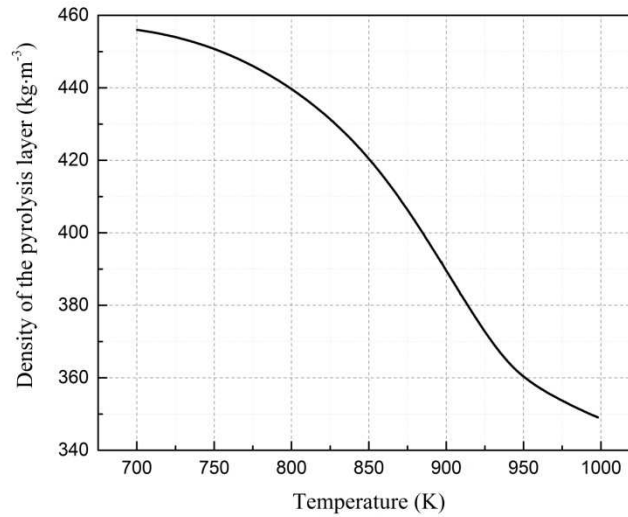

Fig. A. 2. Density distribution of the pyrolysis layer calculated by the thermogravimetry data of the charring material

The specific heat c_{p2} of the pyrolysis layer is acquired from the linear interpolation of those in the virgin layer and the char layer listed in Table A. 1; it is best formulated as a function of temperature

$$c_{p2}(T) = 3.178 \times T - 1651.6 \qquad \text{J·kg}^{-1}\text{·K}^{-1}$$
(A. 2)

References

[1] J. C. Ferguson, F. Panerai, J. Lachaud, Theoretical study on the micro-scale

oxidation of resin-infused carbon ablators, Carbon. 121 (2017) 552-562. http://dx.doi.org/10.1016/j.carbon.2017.06.013.

[2] W. S. Lin, Quasi-steady solutions for the ablation of charring materials, Int. J. Heat. Mass. Tran. 50 (5) (2007) 1196-1201. http://dx.doi.org/10.1016/j. ijheatmasstransfer.2006.11.011.

[3] Y. Tian, H. Huang, X. Xu, Curing kinetics and curing process of phenolic impregnated carbon ablator, J. Appl. Polym. Sci. 134 (42) (2017) 45434. http://dx.doi.org/10.1002/app.45434.

[4] Y. Tian, H. Huang, X. Xu, Optimization of the curing process of phenolic impregnated carbon ablator, J. Appl. Polym. Sci. 135 (18) (2018) 46230. http://dx.doi.org/10.1002/app.46230.

[5] K. Torkashvand, E. Poursaeid, J. Ghazanfarian, Experimental and Numerical Study of Thermal Conductivity of Plasma-Sprayed Thermal Barrier Coatings with Random Distributions of Pores, Appl. Therm. Eng. 137 (2018) 494-503. http://dx.doi.org/10.1016/j.applthermaleng.2018.04.002.

[6] S. Shi, L. Li, J. Liang, Surface and volumetric ablation behaviors of SiFRP composites at high heating rates for thermal protection applications, Int. J. Heat. Mass. Tran. 102 (2016)1190-1198. http: //dx.doi.org/10.1016/j.ijheatmasstransfer. 2016.06.085.

[7] S. L. Mitchell, Applying the combined integral method to one-dimensional ablation, Appl. Math. Model. 36 (1) (2012) 127-138. http: //dx.doi.org/10.1016/

j.apm. 2011.05.032.

[8] S. L. Guo, B.L. Wang, Thermal shock cracking behavior of a cylinder specimen with an internal penny-shaped crack based on non-fourier heat conduction, Int. J. Thermophys. 37 (2) (2016) 1-23. http://dx.doi.org/10.1007/s10765-015-2029-6.

[9] T. Cheng, W. Li, W. Lu, Heattransfer and failure mode analyses of ultrahigh-temperature ceramic thermal protection system of hypersonic vehicles, Math. Probl. Eng. 13-14 (2014) 1-11. http://dx.doi.org/10.1155/2014/412718.

[10] W. C. Park, A. Atreya, H. R. Baum, Determination of pyrolysis temperature for charring materials, P. Combust. Inst. 32 (2) (2009) 2471-2479. http://dx.doi.org/ 10.1016/j.proci.2008.06.060.

[11] T. G. Desai, J. W. Lawson, P. Keblinski, Modeling initial stage of phenolic pyrolysis: graphitic precursor formation and interfacial effects, Polymer. 52 (2) (2011) 577-585. http://dx.doi.org/10.1016/j.polymer.2010.11.018.

[12] W. Li, H. Huang, Y. Tian, Nonlinear analysis on thermal behavior of charring materials with surface ablation, Int. J. Heat. Mass. Tran. 84 (2015) 245-252. http://dx.doi.org/10.1016/j.ijheatmasstransfer.2015.01.004.

[13] W. Li, H. Huang, Y. Tian, A nonlinear pyrolysis layer model for analyzing thermal behavior of charring ablator, Int. J. Therm. Sci. 98 (2015) 104-112. http://dx.doi.org/10.1016/j.ijthermalsci.2015.07.002.

[14] Y. K. Chen, F. S. Milos, Ablation and thermal response program for spacecraft heatshield analysis, J. Spacecraft. Rockets. 36 (3) (1999) 475-483.

http://dx.doi.org/10.2514/2.3469.

[15] Y. K. Chen, F. S. Milos, Effects of nonequilibrium chemistry and darcy—forchheimer pyrolysis flow for charring ablator, J. Spacecraft. Rockets. 50 (2) (2013) 256-269. http://dx.doi.org/10.2514/1.A32289.

[16] R. Fu, H. Weng, J. F. Wenk, A. Martin, Thermomechanical coupling for charring ablators, J. Thermophys. Heat. Tr. 32 (2) (2018) 369-379. http://dx.doi.org/10.2514/1.T5194.

[17] H. W. Wong, J. Peck, J. Assif, Detailed analysis of species production from the pyrolysis of the Phenolic Impregnated Carbon Ablator, J. Anal. Appl. Pyrol. 122 (2016) 258-267. http://dx.doi.org/10.1016/j.jaap.2016.09.016.

[18] S. Shi, F. Yi, S. Tang, A solar radiant heating apparatus for measuring the thermal behavior of silica fiber phenolic composite for thermal protection applications, Appl. Therm. Eng. 106 (2016) 236-243. http://dx.doi.org/10.1016/j.applthermaleng.2016.06.007.

[19] T. Periadurai, C. T. Vijayakumar, M. Balasubramanian, Thermal decomposition and flame retardant behaviour of SiO2-phenolic nanocomposite, J. Anal. Appl. Pyrol. 89 (2) (2010) 244-249. http://dx.doi.org/10.1016/j.jaap.2010.08.010.

[20] J. Scoggins, N. Mansour, H. Hassan, Development of reduced kineticmechanism for PICA pyrolysis products, in: 42nd AIAA Thermophysics Conference, Honolulu, Hawaii, 2011. AIAA 2011-3126. http://dx.doi.org/10.2514/6.2011-3126.

[21] L. Costaa, L. R. diMontelera, G. Caminoa, E. D. Weilb, E. M. Pearce, Structure-charring relationship in phenol-formaldehyde type resins, Polym. Degrad. Stabil. 56 (1) (1997) 23-35. https://doi.org/10.1016/S0141-3910 (96)00171-1.

[22] W. N. dos Santos, J. A. de Sousa, R. Gregorio, Thermal conductivity behaviour of polymers around glass transition and crystalline melting temperatures, Polym. Test. 2 (5) (2013) 987-994. http://dx.doi.org/10.1016/j.polymertesting. 2013.05. 007.

[23] A.Tessema, D. Zhao, J. Moll, Effect of filler loading, geometry, dispersion and temperature on thermal conductivity of polymer nanocomposites, Polym. Test. 57 (2017) 101-106. http://dx.doi.org/10.1016/j.polymertesting.2016.11.015.

[24] I. H. Tavman, Effective thermal conductivity of isotropic polymer composites, Int. J. Heat. Mass. Tran. 25 (5) (1998) 723–732. http://dx.doi.org/10.1016/ s0735-1933 (98)00059-1.

[25] G. L. Delfa, J. Luinge, A. G. Gibson, Next generation composite aircraft fuselage materials under post-crash fire conditions, in: 1st Conference on Engineering Against Fracture, 2009. https://doi.org/10.1007/978-1-4020-9402- 6_14.

[26] M. Muller, S. Bourbigot, S. Duquesne, Investigation of the synergy in intumescent polyurethane by 3D computed tomography, Polym.Degrad. Stabil. 98 (9) (2013)1638-1647. https://doi.org/10.1016/j.polymdegradstab.2013.06.018.

[27] H. Muller, A. A. Howling, C. Hollenstein, Inverse identification of thermal

properties of charring ablators, Numer. Heat. Tr. B-Fund. 56(6) (2010) 478-501.

https://doi.org/10.1080/10407790903508129.

[28] S. Y. Zhao, B. M. Zhang, S. Y. Du, Inverse identification of thermal properties of

fibrous insulation from transient temperature measurements, Int. J. Thermophys.

30 (6) (2009) 2021-2035. https://doi.org/10.1007/s10765-009-0680-5.

Highlights

1. Equipment about thermal conductivity of the pyrolysis layer is designed.

2. Inversion method for thermal conductivity of the pyrolysis layer is presented.

3. Thermal conductivity of the pyrolysis layer is obtained.

4. Pressure has effect on the pyrolysis rate of the charring material.

5. Relationship between thermal conductivity and pressure is revealed.